Pergamon

Int. J. Heat Mass Transfer. Vol. 37, Suppl. 1, pp. 281–289, 1994

0017-9310/94 $6.00+0.00

0017-9310(93)E0048-L

Buoyancy effect on three-dimensional turbulent surface jet

FUMIMARU OGINO and KOSUKE KATAI

Department of Chemical Engineering, Kyoto University, Kyoto 606, Japan

Abstract—A three-dimensional jet of low temperature discharged from a rectangular flume on the horizontal surface of a large water body of higher temperature was investigated experimentally. The longitudinal variations of the location of the jet axis, vertical and lateral widths of the jet and the time-averaged velocity and temperature at the jet axis are well correlated by a scaling law derived from the dimensional analysis of the governing equations and boundary conditions. The vertical and lateral profiles of both the time-averaged velocity and temperature show satisfactory similarity profiles.

1. INTRODUCTION

THE TRANSPORT of heat and momentum in the environment is usually complicated by the effect of buoyancy. A three-dimensional turbulent jet of low temperature discharged from a flume onto the horizontal surface of a large water body of higher temperature is an important flow with significant buoyancy effect.

The three-dimensional heated surface jet has been the subject of many theoretical and experimental studies [1–4]. However, little is known about the three-dimensional surface jet with negative buoyancy even as far as the overall jet structure is concerned. There exist no reliable data on the velocity and temperature profiles.

The purpose of this paper is to present comprehensive experimental results on the longitudinal variations of the location of jet axis, the vertical and lateral widths of the jet, the decay of the time-averaged velocity and temperature at the jet axis, and the velocity and temperature profiles for the jet of low temperature discharged from a flume on the surface of the ambient water of higher temperature.

A new scaling law is also presented by making use of a similar procedure as those in the heated vertical jet [5], in the two-dimensional heated surface jet [6], and in the three-dimensional heated surface jet [4].

2. DIMENSIONAL ANALYSIS

To correlate the experimental data, a new scaling law is derived from the dimensional analysis of the governing equations and the boundary conditions for the three-dimensional horizontal surface jet.

Figure 1 shows the coordinate system for three-dimensional surface buoyant jet of temperature T_0 and velocity U_0 discharged into an ambient with uniform higher temperature of T_∞.

The flow is assumed to be steady, three-dimensional and of the boundary layer type. The equations governing the surface jet are written in the dimensionless form as,

$$\frac{\partial U^*}{\partial x^*}+\frac{\partial V^*}{\partial y^*}+\frac{\partial W^*}{\partial z^*}=0 \tag{1}$$

$$U^*\frac{\partial U^*}{\partial x^*}+V^*\frac{\partial U^*}{\partial y^*}+W^*\frac{\partial U^*}{\partial z^*}=\frac{\partial}{\partial y^*}(-\overline{u^*v^*})+\frac{\partial}{\partial z^*}(-\overline{u^*w^*})+\frac{1}{Fr}\frac{\partial}{\partial x^*}\int_{y^*}^{\infty}T^*\,dy^* \tag{2}$$

$$U^*\frac{\partial W^*}{\partial x^*}+V^*\frac{\partial W^*}{\partial y^*}+W^*\frac{\partial W^*}{\partial z^*}=\frac{\partial}{\partial y^*}(-\overline{v^*w^*})+\frac{\partial}{\partial z^*}(-\overline{w^*w^*})+\frac{1}{Fr}\frac{\partial}{\partial z^*}\int_{y^*}^{\infty}T^*\,dy^* \tag{3}$$

$$U^*\frac{\partial T^*}{\partial x^*}+V^*\frac{\partial T^*}{\partial y^*}+W^*\frac{\partial T^*}{\partial z^*}=\frac{\partial}{\partial y^*}(-\overline{v^*t^*})+\frac{\partial}{\partial z^*}(-\overline{w^*t^*}) \tag{4}$$

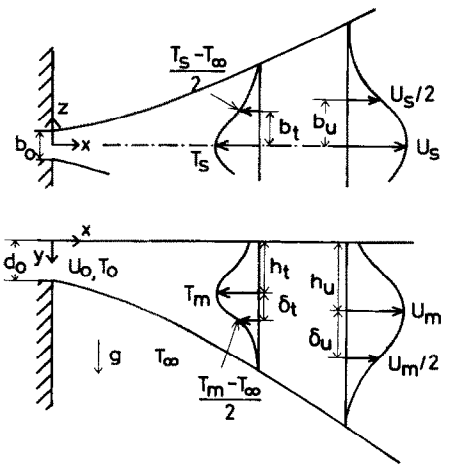

FIG. 1. Three-dimensional surface jet of low temperature.

NOMENCLATURE

b	lateral half-value width of the jet at the surface
b_0	width of the inlet flume
d_0	depth of the water in the inlet flume
Fr	Froude number, $U_0^2/\beta g(T_\infty - T_0)d_0$
g	gravitational acceleration
h	depth of the jet axis
T	time-averaged temperature
U	longitudinal time-averaged velocity
u	longitudinal velocity fluctuation
V	vertical time-averaged velocity
v	vertical velocity fluctuation
W	lateral time-averaged velocity
w	lateral velocity fluctuation
x	longitudinal coordinate
y	vertical coordinate
z	lateral coordinate.

Greek symbols

β	coefficient of volume expansion
δ	vertical half-value width of the jet.

Subscripts

m	value at the jet axis
s	value at the surface
t	temperature
u	velocity
0	value at the jet discharge
∞	value of the ambient.

Superscripts

$\bar{}$	time-averaged value
*	nondimensionalized value by U_0, $T_\infty - T_0$ and d_0
#	normalized value by the scaling law.

where equation (1) is the continuity equation, equations (2) and (3) are momentum equations in the x and z directions, and equation (4) is the thermal energy equation. Density differences have been neglected in all but the buoyancy term (Boussinesq approximation). However, the buoyancy terms in equations (2) and (3) are not direct body force terms but represent, respectively, the streamwise and lateral gradients of excess hydrostatic pressure [1]. The viscous and conductive terms are neglected in equations (2)–(4), since they are small compared with the turbulent stresses and heat fluxes. Furthermore, the viscous dissipation is neglected in equation (4).

The boundary conditions are:

B.C.1 $x^* = 0, \quad 0 < y^* < 1$ and

$$0 < z^* < (b_0/d_0)/2; \quad U^* = 1, \quad T^* = 1 \tag{5a}$$

B.C.1′ $x^* = 0, \quad 1 < y^*$ or $(b_0/d_0)/2 < z^*$;

$$U^* = 0, \quad \partial T^*/\partial x^* = 0 \tag{5b}$$

B.C.2 $y^* = 0; \quad \partial U^*/\partial y^* = 0, \quad \partial T^*/\partial y^* = 0,$

$$V^* = 0 \tag{6}$$

B.C.3 $y^* = \infty; \quad U^* = 0, \quad T^* = 0$ (7)

B.C.4 $z^* = 0; \quad \partial U^*/\partial z^* = 0, \quad \partial T^*/\partial z^* = 0,$

$$W^* = 0 \tag{8}$$

B.C.5 $z^* = \infty; \quad U^* = 0, \quad T^* = 0.$ (9)

If equations (1)–(4) could be solved for U^* and T^* with the boundary conditions (5)–(9) on the assumption that the turbulent stresses and heat fluxes are given as some known functions of x^*, y^* and z^*, the solutions would in principle be of the forms

$$U^* = U^*(x^*, y^*, z^*; Fr, b_0/d_0) \tag{10}$$

$$T^* = T^*(x^*, y^*, z^*; Fr, b_0/d_0). \tag{11}$$

That is, the functional dependence will include all the reduced variables and the one dimensionless number appearing in the differential equations. An additional dimensionless group enters via the foregoing boundary conditions.

Although equations (10) and (11) are exact solutions, the inclusion of the Froude number and the aspect ratio of the flume in the functional form is inconvenient for the present purpose to give a correlation of the decay of surface negative buoyant jet. Therefore, we define the following new variables:

$$U^\# = AU^*, V^\# = AV^*, W^\# = AW^*, u^\# = Au^*,$$
$$v^\# = Av^*, w^\# = Aw^* \tag{12}$$

$$T^\# = BT^*, t^\# = Bt^* \tag{13}$$

$$x^\# = Cx^*, y^\# = Cy^*, z^\# = Cz^* \tag{14}$$

where A, B and C are functions of Fr and b_0/d_0 to be determined.

Substituting equations (12)–(14) into equations (1)–(4) and the boundary conditions (5)–(9), we obtain

$$\frac{\partial U^\#}{\partial x^\#} + \frac{\partial V^\#}{\partial y^\#} + \frac{\partial W^\#}{\partial z^\#} = 0 \tag{15}$$

$$U^\#\frac{\partial U^\#}{\partial x^\#} + V^\#\frac{\partial U^\#}{\partial y^\#} + W^\#\frac{\partial U^\#}{\partial z^\#} = \frac{\partial}{\partial y^\#}(-\overline{u^\# v^\#}) + \frac{\partial}{\partial z^\#}(-\overline{u^\# w^\#}) + \frac{A^2}{BCFr}\frac{\partial}{\partial x^\#}\int_{y^\#}^{\infty} T^\# \mathrm{d}y^\# \tag{16}$$

$$U^\#\frac{\partial W^\#}{\partial x^\#} + V^\#\frac{\partial W^\#}{\partial y^\#} + W^\#\frac{\partial W^\#}{\partial z^\#} = \frac{\partial}{\partial y^\#}(-\overline{v^\# w^\#}) + \frac{\partial}{\partial z^\#}(-\overline{w^\# w^\#}) + \frac{A^2}{BCFr}\frac{\partial}{\partial z^\#}\int_{y^\#}^{\infty} T^\# \mathrm{d}y^\# \tag{17}$$

$$U^{\#}\frac{\partial T^{\#}}{\partial x^{\#}}+V^{\#}\frac{\partial T^{\#}}{\partial y^{\#}}+W^{\#}\frac{\partial T^{\#}}{\partial z^{\#}}$$

$$=\frac{\partial}{\partial y^{\#}}(-\overline{v^{\#}t^{\#}})+\frac{\partial}{\partial z^{\#}}(-\overline{w^{\#}t^{\#}}) \quad (18)$$

B.C.1 $x^{\#}=0,\quad 0<y^{\#}<C$ and

$$0<z^{\#}<C(b_0/d_0)/2;\quad U^{\#}=A,\quad T^{\#}=B \quad (19a)$$

B.C.1′ $x^{\#}=0,\quad C<y^{\#}$ or $C(b_0/d_0)/2<z^{\#}$

$$U^{\#}=0,\quad \partial T^{\#}/\partial x^{\#}=0 \quad (19b)$$

B.C.2 $y^{\#}=0;$

$$\partial U^{\#}/\partial y^{\#}=0,\quad \partial T^{\#}/\partial y^{\#}=0,\quad V^{\#}=0 \quad (20)$$

B.C.3 $y^{\#}=\infty;\quad U^{\#}=0,\quad T^{\#}=0 \quad (21)$

B.C.4 $z^{\#}=0;$

$$\partial U^{\#}/\partial z^{\#}=0,\quad \partial T^{\#}/\partial z^{\#}=0,\quad W^{\#}=0 \quad (22)$$

B.C.5 $z^{\#}=\infty;\quad U^{\#}=0,\quad T^{\#}=0. \quad (23)$

If we put $A^2/BCFr=1$ in equations (16) and (17), the solutions for $U^{\#}$ and $T^{\#}$ include no parameter from the differential equations, but A, B and C enter into them via the boundary conditions at $x^{\#}=0$. Hence, we consider the limiting form of the solutions for large $x^{\#}$ where the boundary condition at $x^{\#}=0$ is not important and replace B.C.1 and 1′ by

B.C.1″ $$\int_0^{\infty}\int_0^{\infty}(U^{\#})^2\mathrm{d}y^{\#}\mathrm{d}z^{\#}$$

$$-\frac{A^2}{BCFr}\int_0^{\infty}\int_0^{\infty}T^{\#}y^{\#}\mathrm{d}y^{\#}\mathrm{d}z^{\#}=\frac{A^2C^2(2Fr-1)}{2Fr}\frac{b_0}{d_0} \quad (24)$$

$$\int_0^{\infty}\int_0^{\infty}U^{\#}T^{\#}\mathrm{d}y^{\#}\mathrm{d}z^{\#}=ABC^2(b_0d_0). \quad (25)$$

Equations (24) and (25) represent, respectively, the momentum and heat balance between $x^{\#}=0$ and $x^{\#}$, and are obtained by integrating equations (16) and (18).

Now, if we assume $A^2/BCFr$ and $A^2\,C^2\,(2Fr-1)\,(b_0/d_0)/(2Fr)$ in equations (24) and $ABC^2\,(b_0/d_0)$ in equation (25) to be unity, we obtain

$$A=(d_0/b_0)^{1/4}[Fr\,(2Fr-1)/2]^{1/4} \quad (26)$$

$$B=(d_0/b_0)^{1/4}[(2Fr-1)^5/32Fr^3]^{1/4} \quad (27)$$

$$C=(d_0/b_0)^{1/4}[8Fr/(2Fr-1)^3]^{1/4}. \quad (28)$$

Thus the limiting forms of the solutions for $U^{\#}$ and $T^{\#}$ at large $x^{\#}$ are:

$$U^{\#}=U^{\#}(x^{\#},y^{\#},z^{\#}) \quad (29)$$

$$T^{\#}=T^{\#}(x^{\#},y^{\#},z^{\#}) \quad (30)$$

where

$$U^{\#}=(d_0/b_0)^{1/4}[Fr\,(2Fr-1)/2]^{1/4}(U/U_0) \quad (31)$$

$$T^{\#}=(d_0/b_0)^{1/4}[(2Fr-1)^5/32\,Fr^3]^{1/4}$$

$$\times[(T-T_\infty)/(T_0-T_\infty)] \quad (32)$$

$$x^{\#}=(d_0/b_0)^{1/4}[8Fr/(2Fr-1)^3]^{1/4}(x/d_0) \quad (33)$$

$$y^{\#}=(d_0/b_0)^{1/4}[8Fr/(2Fr-1)^3]^{1/4}(y/d_0) \quad (34)$$

$$z^{\#}=(d_0/b_0)^{1/4}[8Fr/(2Fr-1)^3]^{1/4}(z/d_0). \quad (35)$$

From equations (29) and (30) the location of the jet axis, the vertical and lateral widths of the jet, and the velocity and temperature at the jet axis can then be described by the functions of $x^{\#}$ only.

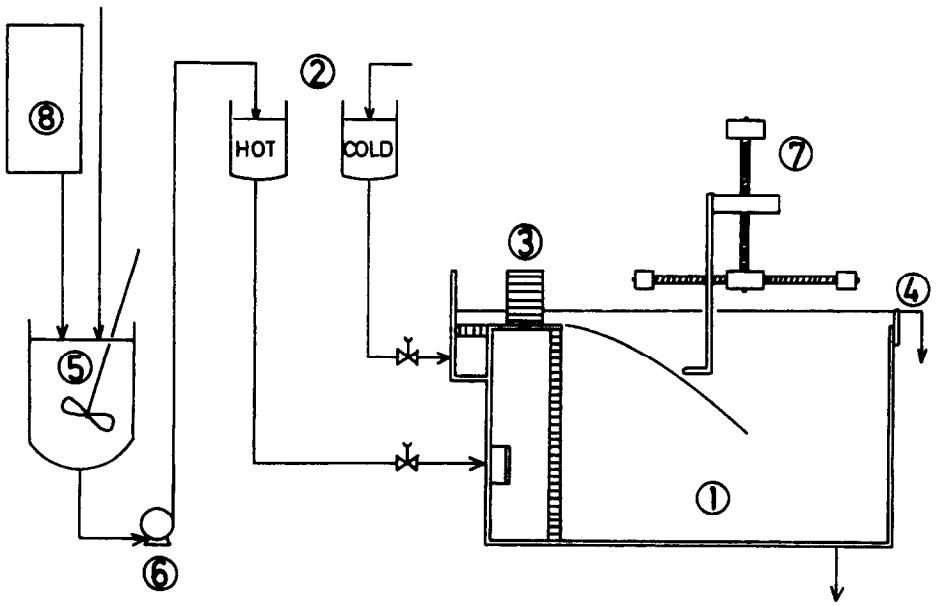

FIG. 2. Schematic drawing of the experimental apparatus: (1) test tank; (2) head tank; (3) honeycomb; (4) overflow weir; (5) mixing tank; (6) pump; (7) traverser; (8) boiler.

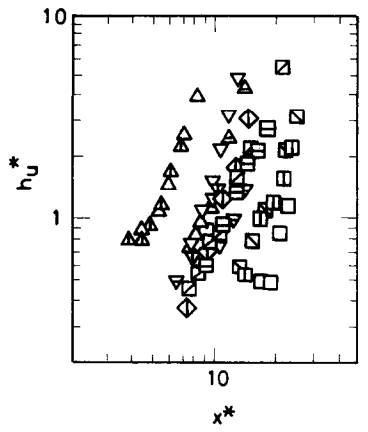

FIG. 3. Longitudinal variation of the location of maximum velocity: △ $Fr = 6$; ▲ $Fr = 8$; ▲ $Fr = 16$; ▽ $Fr = 17$; ▽ $Fr = 27$; ▽ $Fr = 37$; ◇ $Fr = 44$; ◪ $Fr = 55$; ◪ $Fr = 60$; ⊟ $Fr = 62$; ◫ $Fr = 86$; □ $Fr = 148$.

It is interesting to investigate the behavior of the jet when the value of Froude number becomes smaller than 1/2, because the values of A, B and C cannot be determined for $Fr \leqslant 1/2$. In the present experiment we could not reach such a small Froude number.

3. EXPERIMENTAL APPARATUS AND PROCEDURE

The experimental apparatus is shown schematically in Fig. 2. The test tank (1), 2 m long, 1 m wide and 1 m deep, was made of 2.0 cm thick transparent acrylic plates.

Filtered city water which was heated in the heater (8) was used as ambient fluid and its temperature was kept uniform. The ambient water was continuously supplied from a head tank through a screen to prevent the stratification. The velocity of the supplied water was about 5 mm s^{-1} in the test tank.

The jet fluid was also city water the temperature of which was regulated in the tank (2). The water entering the inlet box was passed through a honeycomb (3) equipped at the inlet of a flume and discharged on top of the ambient water to form a three-dimensional surface jet. Two inlet flumes 9.1 and 13.6 mm wide were used. The depth of the flowing water in the flume was controlled by an overflow weir (4) at the downstream end. Flow rate was measured by a calibrated orifice meter.

A series of tests with different temperature of the jet fluid were performed. For each test, measurements of the vertical and lateral widths of the jet and the time-averaged velocity and temperature were made.

The longitudinal velocities were measured with X-type film probe (TSI 1241-20 W) and the temperature with I-type film probe (TSI 1210-20 W) at neighboring locations in the flow. The spacing of these two probes was 1 mm. The velocity signals were obtained by two constant temperature anemometers (DISA 55M10), while the temperature signal was obtained by a constant current anemometer (DISA 55M20) operated as a resistance bridge. The outputs from these anemometers were converted to digital signals with a frequency of 100 Hz and stored in a data recorder (TEAC DR 2000). The sampling time was 170 s. The velocity–temperature calibration curve was then used for calculation of the actual velocity signal from the instantaneous constant temperature anemometer output.

Reynolds numbers based on the hydraulic equivalent diameter at the jet discharge ranged from 1200 to 8000 and the discharge Froude numbers were 6–148. The aspect ratio of the discharged jet at the flume was varied from 0.15 to 0.76.

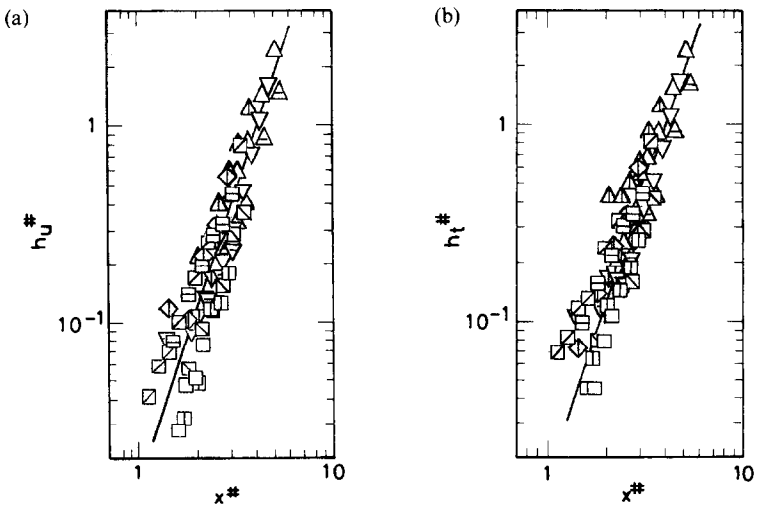

FIG. 4. Longitudinal variations of the locations of maximum velocity and temperature: the symbols are the same as in Fig. 3.

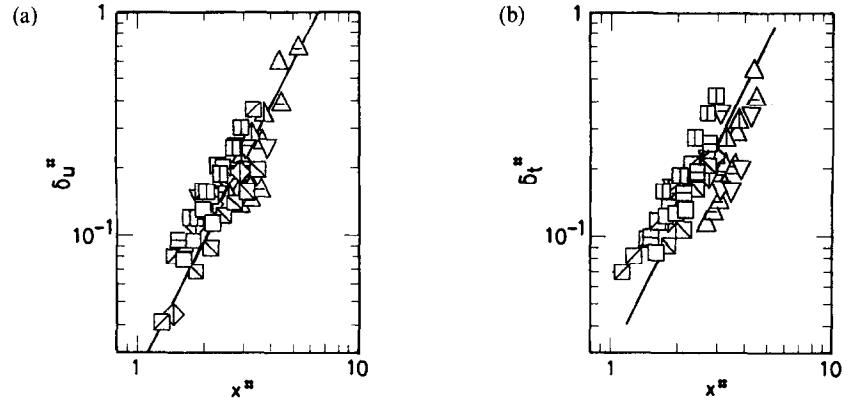

FIG. 5. Longitudinal variation of the vertical half-value width of the jet: the symbols are the same as in Fig. 3.

4. EXPERIMENTAL RESULTS AND DISCUSSIONS

4.1. *Location of jet axis*

The location of the maximum velocity is assumed to be the position of the jet axis. In Fig. 3 the distance of the jet axis from the water surface obtained from the measured velocity profile is plotted against the distance from the jet discharge. Figure 3 shows that the depth of the jet axis seems to vary with the distance from the jet discharge to the power of about 3 and their values increase with decreasing Froude number, that is, increasing buoyancy effect.

The variations of the position of the jet axis scaled with the scaling law obtained in the present analysis with the scaled distance from the jet discharge are depicted in Fig. 4(a). The data points seem to fall on a single line. From Fig. 4(a) the following experimental correlation is obtained for $1 < x^{\#} < 6$.

$$h_u^{\#} = 0.015(x^{\#})^3. \tag{36}$$

In Fig. 4(b) the positions of the maximum temperature deficiency, h_t, are plotted against the distance from the jet discharge. The positions of the maximum temperature deficiency also vary with the distance from the jet discharge to the power of 3 and their values are almost equal to those of the maximum velocity.

4.2. *Width of the jet*

In Fig. 5 vertical half-value width δ_u defined such that $U = U_m/2$ at $y = h_u + \delta_y$ and $z = 0$, and δ_t defined such that $T - T_\infty = (T_m - T_\infty)/2$ at $y = h_t + \delta_t$ and $z = 0$ are plotted against the distance from the jet discharge. The half-value widths of the jet and the distance from the jet source in Fig. 5 are scaled with the scaling law obtained in the present analysis.

Although the scattering of the data on δ_u and δ_t is somewhat large, the data points on δ_u and δ_t seem to fall on single lines. The vertical half-value widths δ_u and δ_t vary roughly in proportion to the square of the distance from the jet discharge. From Figs. 5(a) and (b) the following experimental correlations are obtained for $1 < x^{\#} < 6$.

$$\delta_u^{\#} = 0.024(x^{\#})^2 \tag{37}$$

$$\delta_t^{\#} = 0.030(x^{\#})^2. \tag{38}$$

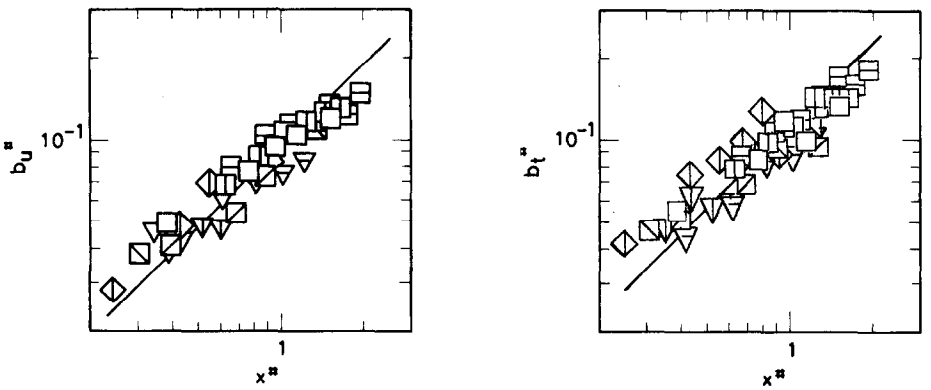

FIG. 6. Longitudinal variation of the lateral half-value width of the jet at the surface: $\nabla Fr = 11$; $\nabla Fr = 22$; $\diamond Fr = 26$; $\boxtimes Fr = 51$; $\boxtimes Fr = 52$; $\boxplus Fr = 68$; $\boxplus Fr = 75$; $\square Fr = 97$.

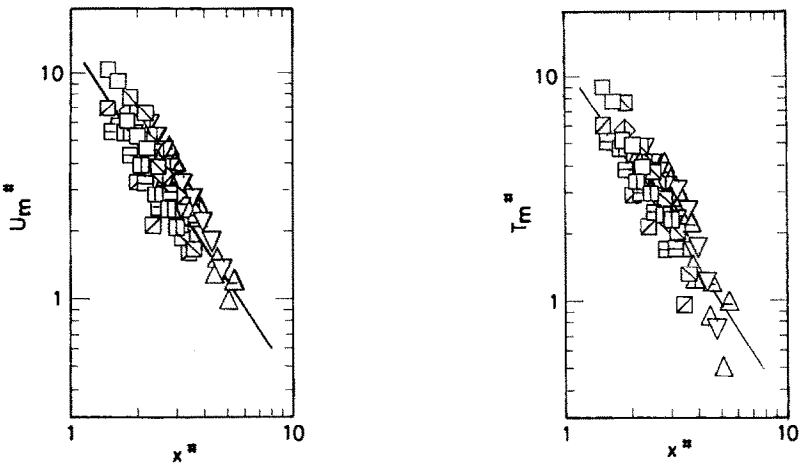

FIG. 7. Decays of the time-averaged velocity and temperature at the jet axis: the symbols are the same as in Fig. 3.

Equations (37) and (38) indicate that the vertical spread of the temperature is a little greater than that of the velocity.

The lateral half-value widths b_u and b_t defined in a similar way to δ_u and δ_t are plotted against x^* in Fig. 6. Both the lateral widths of the jet seem to increase in proportion to the distance from the jet source. The empirical correlation obtained from Fig. 6 is given by

$$b_u^* = 0.1x^* \tag{39}$$

$$b_t^* = 0.12x^*. \tag{40}$$

Comparison between equations (39) and (40) indicates again that the lateral spread of the temperature is larger than that of the velocity.

4.3. *Time-averaged velocity and temperature*

The variations of the time-averaged velocity and temperature at the jet axis with the distance from the jet discharge are shown in Fig. 7.

Figures 7(a) and (b) indicate that the experimental data fall again on single lines for wide range of Froude number. The empirical equations of the time-averaged

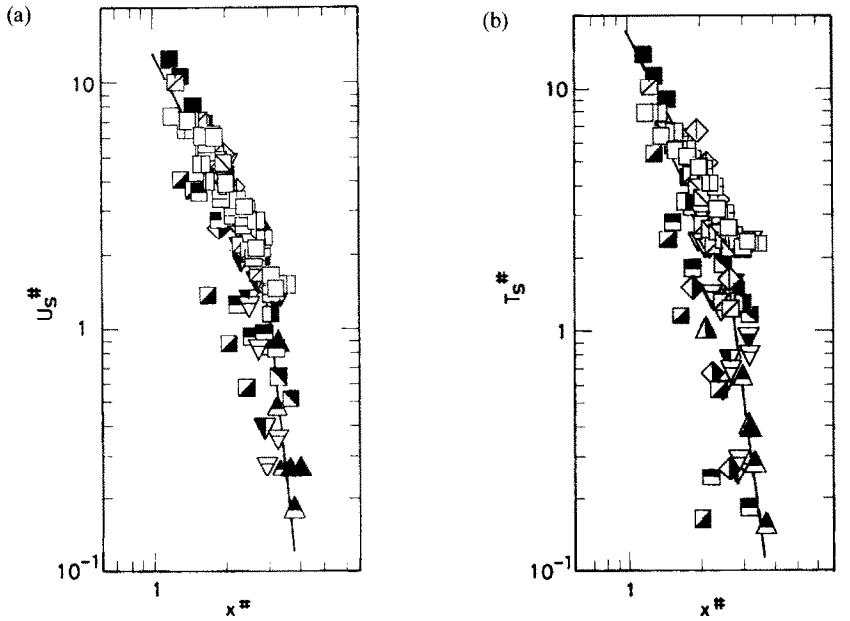

FIG. 8. Decays of the time-averaged velocity and temperature at the surface centerline of the jet: △ $Fr = 8$; △ $Fr = 16$; ▲ $Fr = 17$; ▽ $Fr = 27$; ▽ $Fr = 37$; ◆ $Fr = 44$; ◪ $Fr = 55$; ◹ $Fr = 60$; ◓ $Fr = 62$; ◨ $Fr = 86$; ■ $Fr = 148$; other symbols are the same as in Fig. 6.

velocity and temperature at the jet axis are given by

$$U_m^{\#} = 14(x^{\#})^{-3/2} \tag{41}$$

$$T_m^{\#} = 11(x^{\#})^{-3/2} \tag{42}$$

at

$$1 < x^{\#} < 6.$$

The decays of the time-averaged velocity and temperature at the surface centerline are depicted in Fig. 8. Both the centerline velocity and temperature deficiency decrease with increasing distance from the jet discharge and decreasing rate is noticeable at the region of $x^{\#}$ larger than around 3 where the distance of the jet axis from the surface is roughly twice as large as the vertical half-value width of the jet.

The vertical distributions of the time-averaged velocity and temperature are shown in Figs. 9(a) and (b). The velocity and temperature deficiency are normalized by those at the jet axis and the vertical coordinate y is normalized by the half-value width δ_u and δ_t. The results show similarity profiles of the velocity and temperature which are approximated by Gaus-

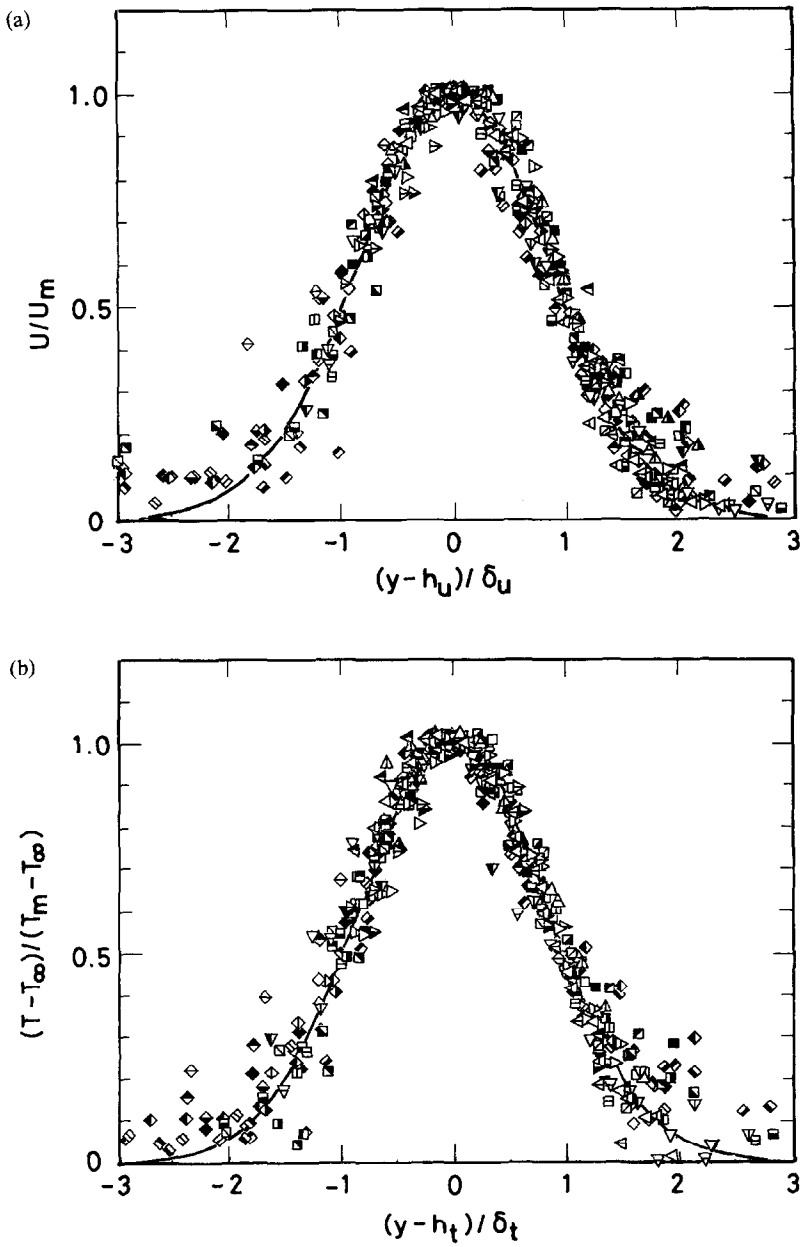

FIG. 9. Vertical distributions of the time-averaged velocity and temperature: ◇◆◆ $Fr = 6$; ◈◈◈ $Fr = 8$; ◈◈◆◆ $Fr = 16$; ◹◹◹ $Fr = 17$; ⊟⊟⊟ $Fr = 27$; ◪◪◪■ $Fr = 37$; ◇◈◈◆ $Fr = 44$; ▽▽▽▽ $Fr = 55$; ▷▷▶▶ $Fr = 60$; □◫◨◧ $Fr = 62$; △◬◬▲ $Fr = 86$; ◁◀◁◀ $Fr = 148$.

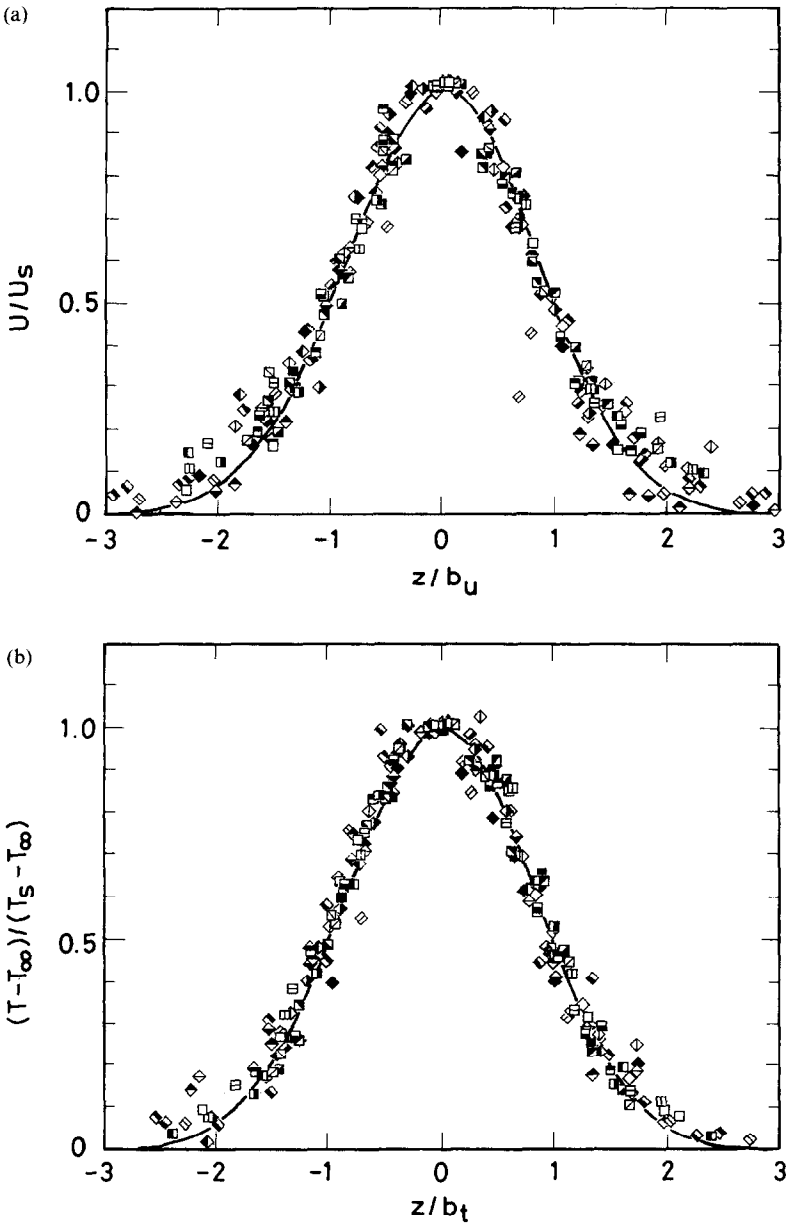

FIG. 10. Lateral distributions of the time-averaged velocity and temperature at the surface: ◇◆◈ $Fr = 11$; ◇◆◆ $Fr = 22$; ◈◓◒◆ $Fr = 26$; ◇◈◈◆◆ $Fr = 55$; ◪◪◩■ $Fr = 52$; ◪◪◩ $Fr = 68$; ◫◓◒ $Fr = 75$; □◫◧◧ $Fr = 97$.

sian distributions as,

$$U/U_m = \exp[-0.69((y-h_u)/\delta_u)^2] \quad (43)$$

$$(T-T_\infty)/(T_m-T_\infty) = \exp[-0.69((y-h_t)/\delta_t)^2]. \quad (44)$$

The lateral distributions of the time-averaged velocity and temperature at the surface are shown in Figs. 10(a) and (b). The results show again the similarity profiles of the velocity and temperature; the empirical equations being

$$U/U_s = \exp[-0.69(z/b_u)^2] \quad (45)$$

$$(T-T_\infty)/(T_s-T_\infty) = \exp[-0.69(z/b_t)^2]. \quad (46)$$

5. CONCLUSIONS

(1) The longitudinal variations of the location of the jet axis, vertical and lateral widths of the jet, and the velocity and temperature at the jet axis are well correlated with the scaling law obtained in the present analysis.

(2) The vertical and lateral distributions of the time-averaged velocity and temperature show similarity profiles.

REFERENCES

1. J. J. McGuirk and W. Rodi, Mathematical modelling of three-dimensional heated surface jets, *J. Fluid Mech.* **95,** 609–633 (1979).
2. G. D. Raithby and G. E. Schneider, The prediction of surface discharge jets by a three-dimensional finite-difference model, *J. Heat Transfer, ASME* **102,** 138–145 (1980).
3. G. H. Jirka, E. E. Adams and K. D. Stolzenbach, Buoyant surface jets, *J. Hydral. Div., Proc. ASCE* **107,** HY11 (1981)
4. F. Ogino, A. Kimoto and M. Kageyama, Transport phenomena in three-dimensional turbulent surface jets with buoyancy effect. In *Transport Phenomena in Turbulent Flows* (Edited by M. Hirata and N. Kasagi), pp. 531–544. Hemisphere, New York (1988).
5. F. Ogino, H. Takeuchi, I. Kudo and T. Mizushina, Heated jet discharged vertically into ambients of uniform and linear temperature profiles, *Int. J. Heat Mass Transfer* **23,** 1581–1588 (1980).
6. F. Ogino, H. Takeuchi, T. Tanaka and T. Mizushina, Buoyancy effect on two-dimensional turbulent surface jet, *Proceedings of the Eighth International Heat Transfer Conference*, Vol. 3, pp. 1177–1182. Hemisphere, Washington, D.C. (1986).